13th International Symposium on Turbulence and Shear Flow Phenomena (TSFP13)
Montreal, Canada, June 25–28, 2024

OPTIMIZING WALL BLOWING FOR GLOBAL SKIN-FRICTION DRAG REDUCTION USING A BAYESIAN OPTIMIZATION FRAMEWORK

Xiaonan Chen
School of Engineering
Newcastle University
Newcastle upon Tyne NE1 7RU, UK
xiaonan.chen@newcastle.ac.uk

Mike Diessner
School of Computing
Newcastle University
Newcastle upon Tyne NE4 5TG, UK
m.diessner2@newcastle.ac.uk

Kevin J. Wilson
School of Mathematics, Statistics and Physics
Newcastle University
Newcastle upon Tyne NE1 7RU, UK
kevin.wilson@newcastle.ac.uk

Richard D. Whalley
School of Engineering
Newcastle University
Newcastle upon Tyne NE1 7RU, UK
richard.whalley@newcastle.ac.uk

ABSTRACT

In this study, low-amplitude wall blowing was employed to reduce the skin-friction drag in zero-pressure-gradient turbulent boundary layers in a wind tunnel. In the first part of the experiment, the global skin-friction drag distribution was measured using a hot-wire at several streamwise positions in the wind tunnel. Generally, the reduction effect of global skin-friction drag is closely linked to the control parameters of wall blowing, including blowing amplitude, frequency, angle, duty cycle, and wavelengths in both the streamwise and spanwise directions. Thus, achieving optimal control strategies to attain the maximum global drag reduction across different Reynolds numbers is equivalent to finding an optimal solution for a complex N-dimensional problem hidden within a black box. In the second part of the experiment, a Bayesian optimization framework (NUBO, Newcastle University Bayesian Optimization) was used to optimize blowing amplitude for maximal local drag reduction. NUBO progressively identified the optimal control strategy to achieve the maximum local drag reduction across various freestream velocities, showing the potential of using this kind of machine learning approach for refined designs in turbulent boundary layer control.

INTRODUCTION

Turbulent boundary layer generated skin-friction drag is prevalent on the surface of high-speed moving trains, airplanes and ships, which results in significant extra energy consumption. For instance, for one A320 type airplane, a 1% drag reduction is expected to reduce the annual operating costs by more than a million dollars (Szodruch, 1991). Controlling the turbulent flow to reduce the skin-friction drag is therefore of great engineering and economic interest. In real-world scenarios, the aforementioned vehicles do not always operate at a constant speed and under constant environmental conditions. Therefore, it becomes necessary to identify different sets of control strategies for a range of Reynolds number cases in order to achieve the maximum drag reduction effect.

A variety of methods used in studies of turbulent boundary layer control show the applicability in skin-friction drag reduction, such as using a dynamic roughness element mounted on the wall (Choi, 1989; Jacobi & McKeon, 2011; Kevin *et al.*, 2017), using a piezoelectric actuator (Bai *et al.*, 2014), using a dielectric barrier discharge plasma actuator (Wang *et al.*, 2013; Chen *et al.*, 2022), using low-amplitude wall-normal microblowing (Hwang, 1997; Kornilov & Boiko, 2012; O'Connor *et al.*, 2023) and so on. To address varying Reynolds number conditions, low-amplitude wall blowing as an active flow control technique which can achieve a long-lasting skin-friction drag reduction effect in the streamwise direction appears to be a feasible choice in the present study. Since the drag reduction effect depends on multidimensional control parameters, including blowing amplitude, frequency, angle, duty cycle, and wavelengths in both the streamwise and spanwise directions, using a machine learning framework to optimize the control strategy might be a potential approach to solving this kind of complex N-dimensional problem. Several previous simulation works (Mahfoze *et al.*, 2019; O'Connor *et al.*, 2023) applied an easy-to-use Bayesian optimization framework (NUBO, Newcastle University Bayesian Optimization (Diessner *et al.*, 2023)) to optimize the control parameters of low-amplitude wall-normal blowing in a turbulent boundary layer flow. In the present study, we aim to employ the same optimization framework, NUBO, to achieve maximal local drag reduction across a large range of Reynolds numbers. This is the first attempt at using NUBO in a wind tunnel as part of a physical fluid dynamics experiment. Once NUBO is proven to work well with our experimental system, it will be applied to optimize more control parameters in further investigations.

EXPERIMENTAL SETUP

The experiment was performed in the boundary layer wind tunnel facility located at Newcastle University. The schematic of the experimental setup is shown in Figure 1. The flat plate used as the wall surface of the turbulent boundary layer is 3.5 m long with a trailing edge flap. To promote the transition to turbulence, a tripping zigzag with a height of 1.5 mm and a width of 10 mm was installed 100 mm downstream of the tip of the flat plate. The origin of the coordinate system is set at the centre of the tripping zigzag. Throughout the paper, we use x, y, and z to refer to the streamwise, wall-normal, and spanwise directions, respectively. The laser drilled microblowing rig has dimensions of 355 mm in length, 290 mm in width, and 1 mm in thickness. It is embedded in the wall with the blowing region set at $x = 475$ mm to $x = 830$ mm. The hole diameter of the microblowing rig is 0.155 mm and 0.08 mm on the top side and bottom side, respectively. The porosity of the microblowing rig is 15.2% on the top side and 5.4% on the bottom side, respectively. To obtain the skin-friction distribution in the turbulent boundary layer with and without the flow control, a hot-wire sensor with a diameter of 0.5 μm and a length of 1.25 mm was employed to measure the near-wall mean velocity profile using a linear-fit technique (Hutchins & Choi, 2002). The hot-wire was driven by a StreamLine Pro anemometer system, with an overheat ratio of 1.5. The measurement data were recorded by a National Instruments data acquisition system. The sampling frequency was 20 kHz and the sampling number was 300,000.

The experiment is divided into two phases. In the first phase, the freestream velocities were set at 6.0 m/s and 21.0 m/s, resulting in Reynolds numbers of $Re_\tau = 390$ and $Re_\tau = 833$ at 5 mm upstream of the blowing region, respectively. At this position, the boundary layer thickness δ_{99} is 22.7 mm for $Re_\tau = 390$ and 18.3 mm for $Re_\tau = 833$. For clarity, the case with a freestream velocity of 6.0 m/s is labeled as the low Reynolds number case, and the case with 21.0 m/s is labeled as the high Reynolds number case in the present study. The mean velocity profiles of the turbulent boundary layers with and without flow control at several different streamwise positions (as denoted by red points in Figure 1) were measured to verify that the boundary layers were fully developed as expected and to assess the global drag reduction level achieved by the wall-normal blowing device.

In the second phase, the wall-normal blowing velocity u_b is considered a controllable parameter, while the free-stream wind speed is considered an environmental variable which is uncontrollable in practice. The wall-normal blowing velocity u_b ranges from 0 m/s to 0.64 m/s. The freestream velocity varies continuously within the range of 5 m/s to 20 m/s. To optimize the flow control strategy for each Reynolds number to achieve the maximum local drag reduction at a position of 5 mm downstream of the blowing region (as denoted by blue star in Figure 1), the local friction velocity u_τ, along with the corresponding wall-normal blowing velocity u_b and free-stream wind speed U_∞, were sent to NUBO as initial inputs. From this, NUBO generated the next controllable parameter u_b for a randomly chosen environmental variable U_∞. After a series of iterations, NUBO should find the optimal control parameter for each Reynolds number. For further information regarding NUBO and its validation, please refer to Diessner *et al.* (2022).

MICROBLOWING DEVICE PERFORMANCE

To assess the uniformity of the wall-normal blowing, a hot-wire was used to measure the blowing velocity on the microblowing rig. It is worth noting that the hot-wire measured blowing velocity u_{bh} is lower than its true value, because the hot-wire cannot physically touch the blowing rig surface. As shown in Figure 2, the x axis and z axis represent the length and width of the microblowing rig, corresponding to the streamwise and spanwise direction of the wind tunnel, respectively. The center of the rig in the spanwise direction is highlighted by the yellow dashed line, along which we take measurements for skin-friction in the turbulent boundary layer. The gray-scale

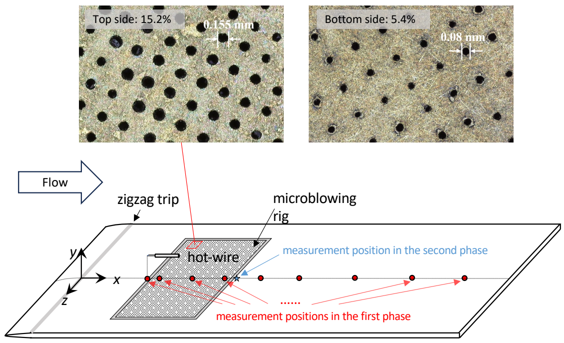

Figure 1: Schematic of the experimental setup.

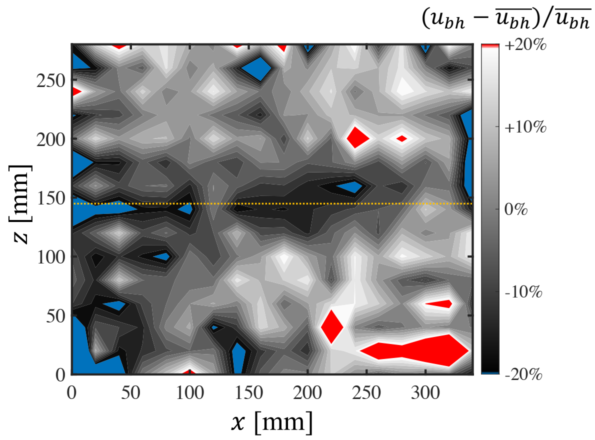

Figure 2: Wall-normal blowing velocity distribution measured on the microblowing rig using a hot-wire.

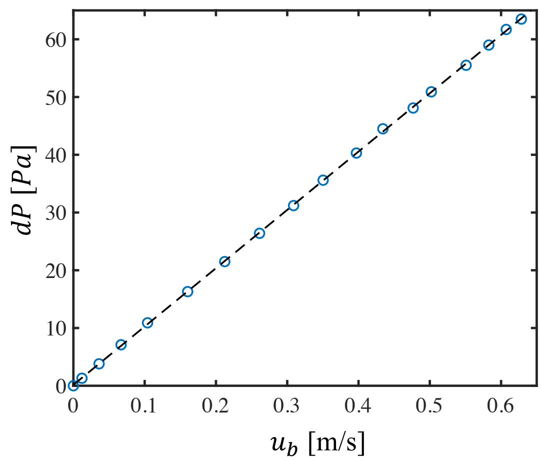

Figure 3: Pressure difference between the microblowing rig pressure chamber and environment.

in the contour map shows the ratio of the difference between the local blowing velocity and the spatially averaged velocity. The red regions and blue regions on the contour map represent areas where the blowing velocity is greater than and less than 20% of the spatially averaged blowing velocity, respectively. It is clear that most areas on the microblowing rig have a uniform blowing velocity fluctuating within 20%.

As shown in Figure 3, the pressure difference between the microblowing rig's pressure chamber and the environment (with freestream velocity $U_\infty = 0$ m/s) was measured by a

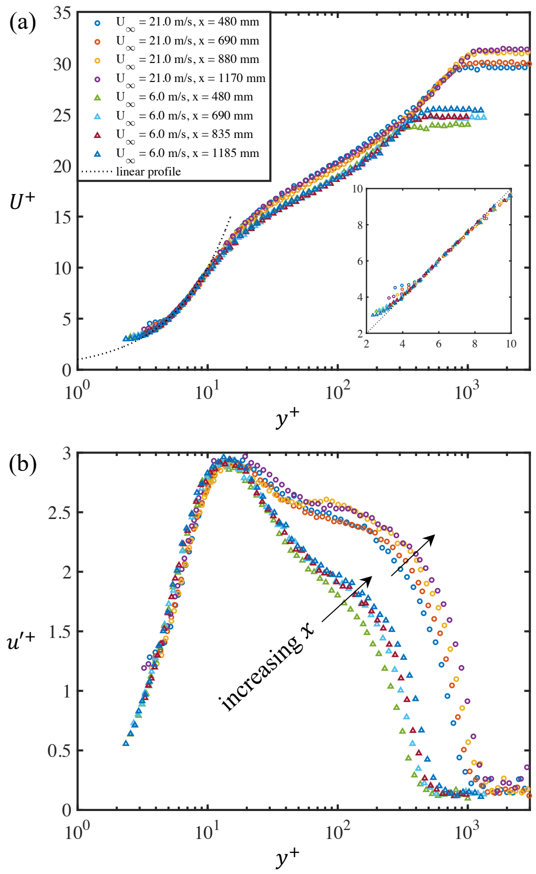

Figure 4: Wall-normal profiles of boundary layer properties: (a) mean velocity profile; (b) streamwise turbulent intensity profile.

manometer. Here, the blowing velocity u_b was calculated based on the measured flow rate using a mass flow meter with an accuracy of $\pm(3\%\ o.m.v. + 0.3\%\ FS)$. Clearly, the pressure drop across the microblowing rig increases linearly with the blowing velocity, indicating that higher blowing velocities result in greater energy consumption.

GLOBAL FLOW CHARACTERIZATION

The boundary layer mean velocity profiles and streamwise turbulent intensity profiles measured at several different streamwise positions without flow control are shown in Figure 4 (a) and (b), respectively. In all cases, the profiles were normalized using the friction velocity u_τ, estimated through a linear fit technique. As shown in Figure 4 (a), the mean velocity profiles fit well with the linear profile in the range of $5 \leq y^+ \leq 7$ and exhibit a clear logarithmic region at higher wall-normal positions. For the streamwise turbulent statistics (Figure 4 (b)), the streamwise turbulent intensity profiles collapse onto each other below $y^+ = 20$ and peak at $y^+ = 15$. An increase in turbulent intensity is observed with increasing streamwise locations in the outer region for both low and high Reynolds number cases. This is because an increase in streamwise locations results in a higher Reynolds number, leading to a greater contribution from large-scale structures (Hutchins & Marusic, 2007; Hutchins *et al.*, 2009).

Figure 5 shows a comparison of the mean velocity profiles of the boundary layer measured under low and high Reynolds number conditions, with and without flow control. The data

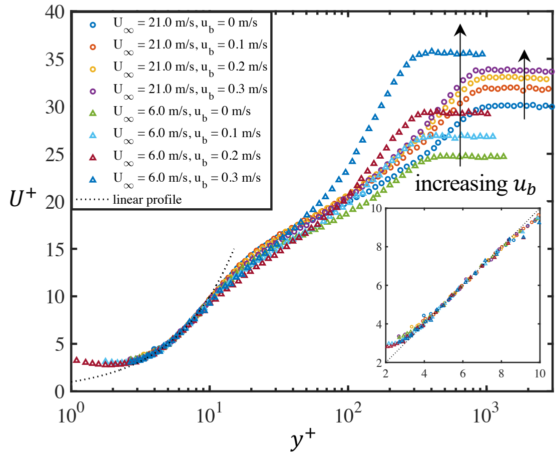

Figure 5: Mean velocity profiles of boundary layer measured under low and high Reynolds number conditions, with and without flow control.

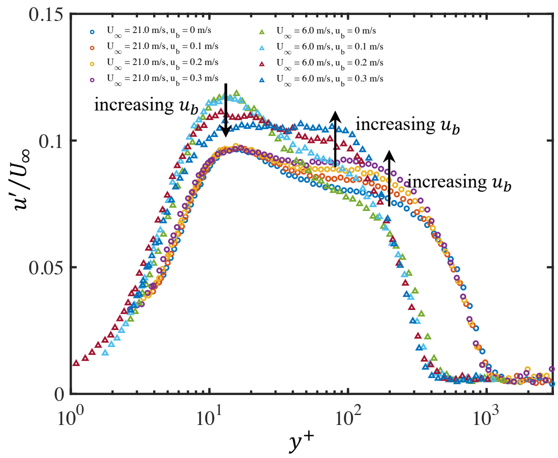

Figure 6: Turbulent intensity profiles of boundary layer measured under low and high Reynolds number conditions, with and without flow control.

were sampled at $x = 690$ mm, around where we obtained the maximum local skin-friction drag reduction with the flow control (see Figure 7). Again, the friction velocities for all cases were estimated using a linear fit technique. For both the low and high Reynolds number cases, the dimensionless mean velocity U^+ in the freestream increases with an increase in wall-normal blowing velocity u_b. This result indicates that a higher level of skin-friction drag reduction will be obtained when u_b is increased. However, for the high Reynolds number case, the change in the dimensionless mean velocity U^+ in the freestream is not as significant as it is in the low Reynolds number case when the blowing velocity is the same. This result suggests that the wall-normal blowing with the same blowing velocity u_b is more effective in reducing the skin-friction at low Reynolds number.

To investigate the effect of wall-normal blowing on the turbulent intensity distribution in an intuitive manner, the turbulent intensity profiles normalized using U_∞ were plotted as shown in Figure 6. For the low Reynolds number case, the turbulent intensity of the inner peak decreases, while the turbulent intensity of the outer peak increases with an increase in wall-blowing velocity. For the high Reynolds number case, the tur-

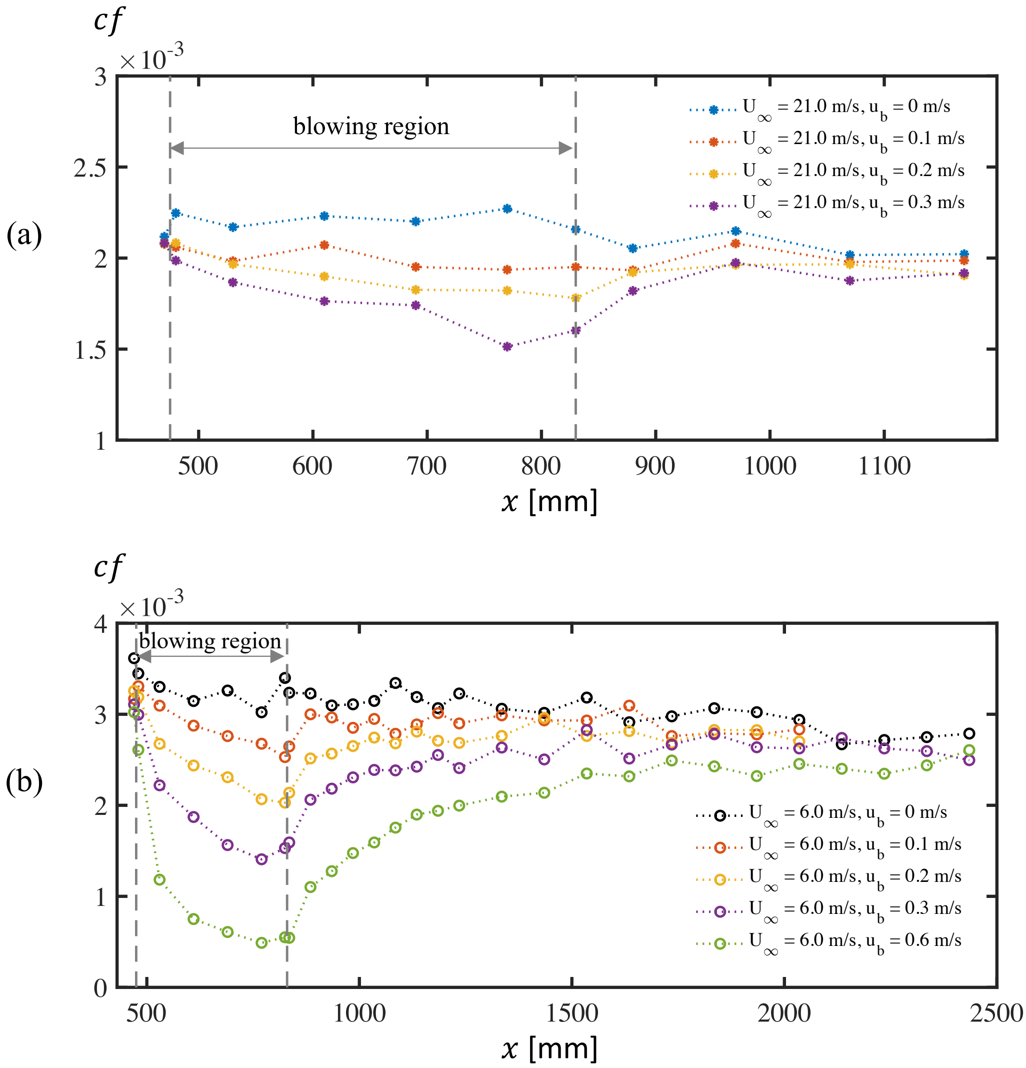

Figure 7: Streamwise skin-friction coefficient distribution with and without flow control. (a) measured at $U_\infty = 21.0$ m/s; (b) measured at $U_\infty = 6.0$ m/s.

U_∞ [m/s]	6.0				21.0		
u_b [m/s]	0.09	0.19	0.32	0.64	0.11	0.21	0.32
$C_B = u_b/U_\infty$	0.015	0.031	0.053	0.106	0.005	0.010	0.015
$\overline{C_{f0}}$	0.003				0.0021		
$\overline{C_{fb}}$	0.0029	0.0027	0.0024	0.0019	0.0020	0.0019	0.0018
$GDR = (\overline{C_{f0}} - \overline{C_{fb}})/\overline{C_{f0}}$	5.2%	12.5%	20.6%	37.2%	7.1%	10.97%	15.8%

Table 1: A summary of experimental conditions with corresponding wall-normal blowing parameters and global skin-friction drag reduction (%).

bulent intensity profiles in the near-wall region collapse, while the turbulent intensity in the outer region increases with an increase in wall-blowing velocity. Similar results for the change in the outer region were also observed by Chen *et al.* (2022), who used a plasma actuator to generate wall-normal blowing in a turbulent boundary layer. The increase in turbulent intensity in the outer region was explained by the near-wall high-turbulence fluid being lifted by the wall-normal blowing (Chen *et al.*, 2022). For the change in the inner region, the result suggests that only a massive skin-friction drag reduction could lead to the suppression of the inner peak of turbulent intensity.

GLOBAL SKIN-FRICTION DRAG REDUCTION

Figure 7 (a) and (b) show the streamwise distribution of the skin-friction coefficients measured with and without flow control, under high and low Reynolds number conditions, respectively. For both cases, the skin-friction coefficient decreases gradually with increasing streamwise positions in the absence of control, exhibiting classic characteristics of a canonical turbulent boundary layer. For the flow control cases, the skin-friction coefficient decreases significantly from the region where wall-normal blowing begins and gradually recovers to match the non-blowing case downstream of the blowing region. This result implies that the wall-normal blowing used in this study has achieved a long-lasting drag reduction effect in the streamwise direction. However, compared to the low Reynolds number cases, the recovery of the skin-friction coefficient for the high Reynolds number cases is much quicker when the same blowing amplitude was applied. For clarity, the drag reduction effect extends at least $38\delta_{99}$ in the streamwise direction for the high Reynolds number case, and $87\delta_{99}$ for the low Reynolds number case. Here, δ_{99} represents the boundary layer thickness measured at 5 mm upstream of the blowing region. This is consistent with the aforementioned result that the wall-normal blowing with the same blowing velocity u_b is more effective in reducing the skin-friction at low Reynolds number.

With the increase in the intensity of wall-normal blowing, the reduction in the global skin-friction coefficient becomes more remarkable. To evaluate the skin-friction drag reduction effect, the global skin-friction drag reduction (*GDR*) was calculated. The corresponding results are summarised in Table 1. For all cases, a positive *GDR* value exists. It is worth noting that Kornilov & Boiko (2012) used a similar microblowing device and achieved an 8.3% global drag reduction with a small blowing coefficient of $C_B = 0.00289$ at $U_\infty = 21 m/s$. This could be attributed to the fact that the porosity of the microblowing plate in the present study was only 15.2% for the top side and 5.4% for the bottom side, respectively, while it was 17.1% on both sides in their study.

OPTIMIZING WALL BLOWING WITH NUBO

Significant global drag reduction was confirmed in both low and high Reynolds number cases. To assess the applicability of NUBO, the first experiment using NUBO was designed to optimize one-dimensional control parameters, i.e., blowing velocity u_b, to obtain the minimum local friction velocity under a range of randomly changing freestream velocities U_∞. Here, the randomly changing freestream velocities are used to simulate real-world scenarios, i.e., a vehicle does not always operate at a constant speed and under constant environmental conditions. Since NUBO requires many data points to optimize control parameters for various wind speeds, we planned to place the hot-wire probe close to the wall to ensure it is in the linear region under this range of wind conditions ($5 \leq U_\infty \leq 20$ m/s). To do so, the near-wall mean velocity profiles were measured across a wide range of freestream velocity conditions. As shown in Figure 8, the linear region for higher freestream velocities exists at locations relatively closer to the wall. The linear regions at the highest ($U_\infty = 19.2$ m/s) and lowest ($U_\infty = 5.1$ m/s) tested velocities do not even overlap. The linear region for low freestream velocity conditions is not observed as close to the wall as for high freestream velocity conditions, which is attributed to the more dominant wall cooling effect under low freestream velocity conditions. Therefore, in the NUBO experiment, if the randomly chosen freestream velocity falls within the range of $5 \leq U_\infty \leq 12$ m/s, the hot-wire probe is fixed at $y = 0.27$ mm. Conversely, if the freestream velocity is between $12 < U_\infty \leq 20$ m/s, the probe is set at $y = 0.18$ mm.

In the experiment with NUBO, a local friction velocity u_τ with a corresponding blowing amplitude u_b and a freestream velocity U_∞ were sent to NUBO as initial inputs. Based on

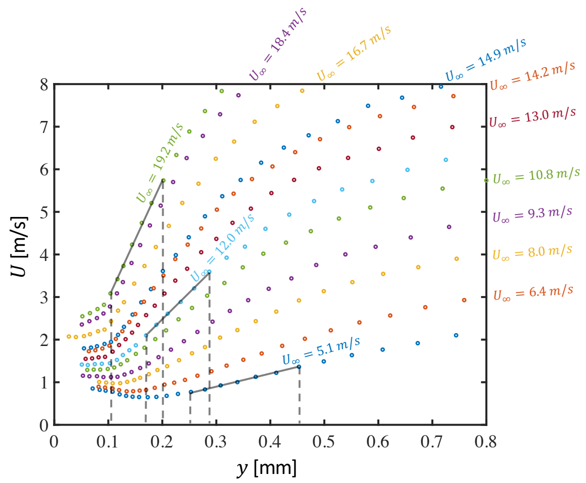

Figure 8: Near-wall mean velocity profiles measured at $x = 835$ mm at different freestream velocities.

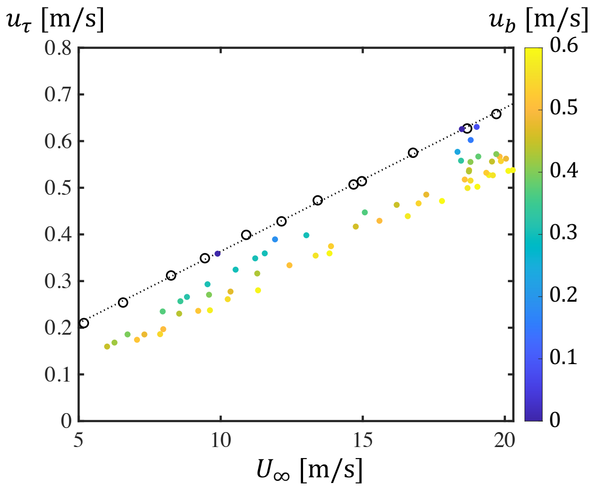

Figure 9: Friction velocities measured at $X = 835$ mm under different freestream velocities and flow control conditions as provided by NUBO. Black circles represent the results measured without flow-control. Colored dots represent the results measured with flow-control.

the inputs, NUBO generates the next controllable parameter u_b for a randomly chosen freestream velocity U_∞. As shown in Figure 9, the colored dots represent the friction velocities measured at $X = 835$ mm (marked by blue star in Figure 1) under 60 sets of randomly chosen freestream velocities and flow control conditions provided by NUBO. The black circles represent the friction velocities measured without flow-control at the same streamwise position for comparison. For no-blowing cases, the friction velocity increases linearly with the increase in freestream speed. For cases with blowing, all measured friction velocity values exist under the fitted curve for the no-blowing case (the dotted line in Figure 9), suggesting a drag reduction effect.

As shown in Figure 10, the black cross marks represent the points input to NUBO, while the contour map represents the drag reduction level which was normalized by the maximum drag reduction level found in each wind speed condition. In the experiment, after a series of iterations, NUBO consistently recommended a high blowing amplitude for each

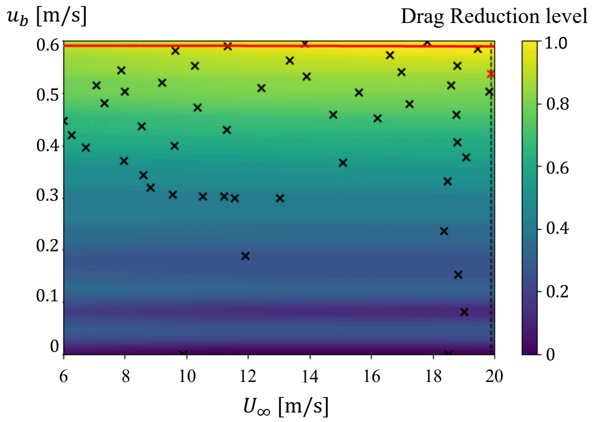

Figure 10: Optimisation of a 2-dimensional problem with one uncontrollable environmental variable U_∞ and one controllable variable u_b. Black cross marks represent the training points. Red cross mark represents the next controllable parameter for the next randomly chosen environmental variable (black dashed line).

randomly determined freestream velocity as indicated by the red line in Figure 10. This outcome suggests that NUBO progressively identified the optimal control strategy to achieve the lowest local friction velocity across various freestream velocities.

CONCLUSION AND OUTLOOK

In this study, we experimentally achieved a reduction in global skin-friction drag in turbulent boundary layers using low-amplitude wall blowing. The initial results indicate that our blowing rig can indeed generate uniform blowing and adjust the blowing intensity as we anticipated, leading to drag reduction effects at different levels. The drag reduction effect extends at least $38\delta_{99}$ in the streamwise direction for the high Reynolds number case, and $87\delta_{99}$ for the low Reynolds number case. Additionally, the maximum global drag reductions achieved for high and low Reynolds numbers are 37.2% and 15.8%, respectively. We have also attempted the very first optimization experiment using NUBO to obtain the lowest local friction velocity across various freestream velocities. As a result, NUBO quickly found the optimal control strategy as we expected, i.e., blowing at a high amplitude within the parameter bounds. While we have currently only achieved drag reduction through varying intensities of uniform wall-normal blowing, we have plans for further modifications. Control parameters, including blowing amplitude, frequency, angle, duty cycle, wavelength will be explored and optimized with NUBO in subsequent experiments to achieve both global skin-friction drag reduction and net energy savings. We plan to conduct a direct numerical simulation (DNS) to validate our experimental results and provide detailed flow field information for further analysis to understand mechanism behind the relationship between control parameters and drag reduction, providing insights for refined design in turbulent boundary layer control. The corresponding results will be presented in future work.

ACKNOWLEDGEMENTS

The present study was supported by the Engineering and Physical Sciences Research Council (EPSRC) under grant numbers EP/T020946/1, EP/T021144/1 and the EPSRC Centre for Doctoral Training in Cloud Computing for Big Data under grant number EP/L015358/1.

REFERENCES

Bai, H. L., Zhou, Y., Zhang, W. G., Xu, S. J., Wang, Y. & Antonia, R. A. 2014 Active control of a turbulent boundary layer based on local surface perturbation. *Journal of Fluid Mechanics* **750**, 316–354.

Chen, X., Iwano, K., Sakai, Y. & Ito, Y. 2022 Effect of artificial large-scale structures on bursting phenomenon in turbulent boundary layer. *Physics of Fluids* **34** (8), 085128.

Choi, K. 1989 Near-wall structure of a turbulent boundary layer with riblets. *Journal of Fluid Mechanics* **208**, 417–458.

Diessner, M., O'Connor, J., Wynn, A., Laizet, S., Guan, Y., Wilson, K. J. & Whalley, R. D. 2022 Investigating Bayesian optimization for expensive-to-evaluate black box functions: Application in Fluid Dynamics. *Frontiers in Applied Mathematics and Statistics* **8**.

Diessner, M., Wilson, K. J. & Whalley, R. D. 2023 NUBO: A transparent Python package for Bayesian optimisation. *arXiv preprint arXiv:2305.06709* pp. 1–21 [submitted to Journal of Statistical Software].

Hutchins, N. & Choi, K. 2002 Accurate measurements of local skin friction coefficient using hot-wire anemometry. *Progress in Aerospace Sciences* **38** (4-5), 421–446.

Hutchins, N. & Marusic, I. 2007 Evidence of very long meandering features in the logarithmic region of turbulent boundary layers. *Journal of Fluid Mechanics* **579**, 1–28.

Hutchins, N., Nickels, T. B., Marusic, I. & Chong, M. S. 2009 Hot-wire spatial resolution issues in wall-bounded turbulence. *Journal of Fluid Mechanics* **635** (2009), 103–136.

Hwang, D. P. 1997 A proof of concept experiment for reducing skin friction by using a micro-blowing technique. In *35th Aerospace Sciences Meeting and Exhibit*. Reno,NV,U.S.A.: American Institute of Aeronautics and Astronautics.

Jacobi, I. & McKeon, B. J. 2011 Dynamic roughness perturbation of a turbulent boundary layer. *Journal of Fluid Mechanics* **688**, 258–296.

Kevin, Monty, J. P., Bai, H. L., Pathikonda, G., Nugroho, B., Barros, J. M., Christensen, K. T. & Hutchins, N. 2017 Cross-stream stereoscopic particle image velocimetry of a modified turbulent boundary layer over directional surface pattern. *Journal of Fluid Mechanics* **813**, 412–435.

Kornilov, V. I. & Boiko, A. V. 2012 Efficiency of air microblowing through microperforated wall for flat plate drag reduction. *AIAA Journal* **50** (3), 724–732.

Mahfoze, O. A., Moody, A., Wynn, A., Whalley, R. D. & Laizet, S. 2019 Reducing the skin-friction drag of a turbulent boundary-layer flow with low-amplitude wall-normal blowing within a bayesian optimization framework. *Physical Review Fluids* **4** (9), 094601.

O'Connor, J., Diessner, M., Wilson, K. J., Whalley, R. D., Wynn, A. & Laizet, S. 2023 Optimisation and analysis of streamwise-varying wall-normal blowing in a turbulent boundary layer. *Flow, Turbulence and Combustion* **110** (4), 993–1021.

Szodruch, J. 1991 Viscous drag reduction on transport aircraft. In *29th Aerospace Sciences Meeting*. Reno,NV,U.S.A.: American Institute of Aeronautics and Astronautics.

Wang, J., Choi, K., Feng, L., Jukes, T. N. & Whalley, R. D. 2013 Recent developments in DBD plasma flow control. *Progress in Aerospace Sciences* **62**, 52–78.